Journal of Alloys and Compounds 1010 (2025) 177010

Contents lists available at ScienceDirect

Journal of Alloys and Compounds

journal homepage: www.elsevier.com/locate/jalcom

Structural, vibrational, and electrical study of the topological insulator $PbBi_2Te_4$ at high pressure

Tania Garcia-Sanchez [a,*,1], Vanesa Paula Cuenca-Gotor [b,2], Hussien H. Osman [c], Alfonso Muñoz [d,3], Plácida Rodriguez-Hernandez [d,4], Juán Ángel Sans [b,5], Samuel Gallego-Parra [e,6], Catalin Popescu [f,7], Oliver Oeckler [g,8], Daniel Errandonea [c,9], Francisco Javier Manjón [b,10]

[a] Departamento de Ingeniería Eléctrica, MALTA Consolider Team, Universitat Politècnica de València, Camino de Vera, s/n., Valencia 46022, Spain
[b] Instituto de Diseño para la Fabricación y Producción Automatizada, MALTA Consolider Team Universitat Politècnica de València, Camino de Vera, s/n., Valencia 46022, Spain
[c] Departamento de Física Aplicada-ICMUV, MALTA Consolider Team, Universitat de València, Dr. Moliner 50, Burjassot, Valencia 46100, Spain
[d] Departamento de Física, MALTA Consolider Team, Universidad de La Laguna, Avenida Astrofísico Francisco Sánchez, s/n, San Cristobal de La Laguna, Tenerife, 38200, Spain
[e] European Synchrotron Radiation Facility, Avenue des Martyrs, 71, Grenoble 38043, France
[f] ALBA-CELLS, MALTA Consolider Team, Carrer de la Llum 2-26, Cerdanyola del Valles, Barcelona 08290, Spain
[g] Institut für Mineralogie, Kristallographie und Materialwissenschaft, Scharnhorststraße 20, Leipzig 04275, Germany

ARTICLE INFO

Keywords:
$PbBi_2Te_4$
Topological insulators
Thermoelectric materials
Tetradymite
High pressure

ABSTRACT

We report a joint experimental and theoretical study of the structural, vibrational, and electric properties of the topological insulator $PbBi_2Te_4$ under compression through X-ray diffraction, Raman scattering, and electrical measurements at high pressure, which are complemented with theoretical calculations that include the analysis of the topological electron density. The internal polyhedral compressibility of the rhombohedral phase, the behavior of its Raman-active modes, the electrical behavior, and the nature of its different bonds under compression are discussed and compared with their parent binary compounds and with related ternary materials. Interestingly, $PbBi_2Te_4$ retains its topological insulating properties as far as the rhombohedral tetradymite-like phase is retained under compression, unlike other tetradymite-like compounds. In addition, $PbBi_2Te_4$ undergoes an unconventional reversible pressure-induced decomposition into the high-pressure phases of its parent binary compounds (PbTe and Bi_2Te_3) above 8 GPa. Finally, we discuss that the intralayer bonds in the tetradymite-like structure of $PbBi_2Te_4$ are electron-deficient multicenter bonds; i.e. bonds of the same kind as those present in its parent binary compounds, in related chalcogenides, such as $SnSb_2Te_4$, and in general in chalcogenide-based phase change materials. These unconventional bonds are intermediate between covalent and metallic bonds and provide exceptional properties to the materials.

* Corresponding author.
E-mail addresses: tagarsan@die.upv.es (T. Garcia-Sanchez), vacuego@fis.upv.es (V.P. Cuenca-Gotor), hussien.helmy@uv.es (H.H. Osman), amunoz@ull.edu.es (A. Muñoz), plrguez@ull.edu.es (P. Rodriguez-Hernandez), juasant2@upvnet.upv.es (J.Á. Sans), samuel.gallego-parra@esrf.fr (S. Gallego-Parra), cpopescu@cells.es (C. Popescu), oliver.oeckler@gmx.de (O. Oeckler), daniel.errandonea@uv.es (D. Errandonea), fjmanjon@fis.upv.es (F.J. Manjón).
[1] 0000-0001-5762-5325
[2] 0000-0003-0819-8528
[3] 0000-0002-5302-5119
[4] 0000-0002-4148-6516
[5] 0000-0001-9047-3992
[6] 0000-0001-6516-4303
[7] 0000-0001-6613-4739
[8] 0000-0003-0149-7066
[9] 0000-0003-0189-4221
[10] 0000-0002-3926-1705

https://doi.org/10.1016/j.jallcom.2024.177010
Received 29 July 2024; Received in revised form 18 September 2024; Accepted 11 October 2024
Available online 17 October 2024

1. Introduction

Since the start of this millennium, there has been a steady increase in the rate of materials consumption obtained directly from the earth (non-renewable materials), so we are forced to look for new compounds to cover our energy needs. In the last decade, new advanced functional compounds have emerged, such as halide perovskite-based solar absorbers, topological insulators, and hydrides for high-temperature superconductivity, [1-6] which can help decrease the rate of materials consumption to cover our energy needs.

Ternary compounds of the $A^{IV}B_2^VX_4^{VI}$ family (A= Ge, Sn, Pb; B= Bi, Sb; X= Se, Te) with a tetradymite-like structure have attracted considerable interest as potential topological insulators (TIs) and topological superconductors (TSs). Shelimova et al. [7,8] These layered materials are very interesting in the materials science field due to their relationship to fundamental physics and their applications in spintronics, [9] quantum computation low power electronics, and phase-change materials. Qi and Zhang [10-15] Moreover, the preservation of the layered tetradymite-like structure for very different compositions opens up considerable opportunities to improve the known properties and discover new emerging properties [16].

$PbBi_2Te_4$ is known as mineral rucklidgeite since it was first observed in Canada mountains [17-19] and is one of the tetradymite-like ternary compounds of the $A^{IV}B_2^VX_4^{VI}$ family. The structural and vibrational properties of this compound have been characterized by X-ray diffraction (XRD) [20-23] and Raman scattering [24] measurements at room pressure and different temperatures. In addition, the electrical properties of this compound have been studied via transport measurements. Zhang and Singh [25-29]. Finally, it must be mentioned that its electronic structure and thermoelectric properties have been widely investigated to determine its capacity as a thermoelectric converter. Kuznetsova et al. [21,25,30,31,29] In fact, n(PbTe)-m(Bi_2Te_3) compounds with n and m integer numbers, such as Bi_2Te_3 (n=0,m=1), $PbBi_2Te_4$ (n=1,m=1), and $PbBi_4Te_7$ (n=1,m=2), have been recently considered as promising thermoelectric materials in a wide temperature range, where the thermoelectric properties depend on the sequence of PbTe and Bi_2Te_3 blocks aligned along the c-axis of the hexagonal unit cell as in a LEGO playset. [25] Moreover, an increase in the thermoelectric Seebeck coefficient has been predicted for this family of LEGO thermoelectrics on increasing compressive strain. [30]

It is well known that chemical bonding is the primary factor that governs the structure and, hence, the properties of a compound. Consequently, a detailed understanding of chemical bonding is necessary in order to design new materials for innovative applications. Wuttig et al. [6] In this context, the investigation of materials properties at high pressure (HP) is a very interesting field since pressure allows the tuning of the interatomic distances that alters the interatomic interactions. This strategy has proved very fruitful to know many materials properties, e.g. the recent discovery of electron-deficient multicenter bonding in pnictogens, chalcogens, and phase change materials. Osman et al. [32,33]

The properties of several TIs of the $A^{IV}B_2^VX_4^{VI}$ family (A= Ge, Sn, Pb; B= Bi, Sb; X= Se, Te) have been studied under compression. HP studies have been conducted in rocksalt-type $SnSb_2Te_4$ and $GeSb_2Te_4$, [34] and more recently in rhombohedral $SnBi_2Te_4$, [35] $PbBi_2Te_4$, [36] $SnSb_2Te_4$, [15] and $GeBi_2Te_4$. Liu et al. [37] A pressure-induced amorphization (PIA) was reported in rocksalt-type $SnSb_2Te_4$ ($GeSb_2Te_4$) upon compression above 11 (15) GPa. [34] A pressure-induced electronic topological transition (ETT) has been suggested to occur in rhombohedral $SnBi_2Te_4$. Hsieh et al. [35] An isostructural phase transition around 2 GPa, a Fermi resonance around 3.5 GPa, and a pressure-induced decomposition into the high-pressure phases of its parent binary compounds (α-Sb_2Te_3 and SnTe) has been reported above 7 GPa in $SnSb_2Te_4$. Sans et al. [15] Moreover, a trial for the rationalization of pressure-induced effects upon the classification of the different $A^{IV}B_2^VX_4^{VI}$ compounds depending on the quadratic elongation of the AX_6 and BX_6 polyhedral units was performed in Ref. [15]. However, the number of HP studies in compounds of this family is still scarce to do such kind of deductions. In addition, many questions have yet to be addressed for the rhombohedral phases of these compounds, like the behavior of the topological properties under compression and, perhaps the most intriguing one, the origin of the pressure-induced superconductivity found in rhombohedral $PbBi_2Te_4$ [36], in $SnSb_2Te_4$, [38] and in $GeBi_2Te_4$. Liu et al. [37]

In this work, we report the behavior of room-temperature structural, vibrational, and electrical properties of $PbBi_2Te_4$ under compression in a combined experimental and theoretical study, where powder X-ray diffraction (XRD), Raman scattering (RS), and transport measurements under high pressure are complemented with ab initio calculations and a thorough electron density analysis. We pay special attention to the evolution of the interlayer van der Waals interaction under compression, considering this feature the key element to understanding the behavior of the c/a ratio under compression and the stability pressure range of its low-pressure (LP) phase. We report that the topological properties of the rhombohedral LP phase of $PbBi_2Te_4$ are retained under compression up to 8 GPa, where we find a reversible pressure-induced chemical decomposition of $PbBi_2Te_4$ into the HP phases of its parent binary compounds (PbTe and Bi_2Te_3). This pressure-induced decomposition explains the appearance of pressure-induced superconductivity reported by previous studies. Moreover, we provide evidence that the extraordinary properties of the LP phase of $PbBi_2Te_4$ are related to the existence of electron-deficient multicenter bonding. This bonding, already present in rocksalt-like phase change materials of the IV-VI semiconductor family, such as PbTe, and in the tetradymite-like structure of pnictogen sesquichalcogenides, such as Bi_2Te_3, makes $PbBi_2Te_4$ a highly-desired multifunctional material. Osman et al. [32,33]

2. Experimental details

Bulk samples of $PbBi_2Te_4$ were prepared by melting stoichiometric amounts of the pure elements Pb (99.999 %, Smart Elements), Bi (99.999 %, Smart Elements) and Te (99.999 %, Alfa Aesar) at 950 °C for 93 h in sealed silica glass ampules under argon atmosphere and subsequent annealing at 450–500 °C for 8 days and then quenched in air. Oeckler et al. [39] Representative parts of the samples were crushed to powders and fixed on Mylar foils with silicon grease to collect powder diffraction patterns on a Huber G670 powder diffractometer equipped with an imaging plate detector (Cu–K $_{\alpha 1}$ radiation, Ge monochromator, λ = 1.54051 Å) in Guinier geometry. Rietveld refinement of powder X-ray diffraction data confirmed the high purity of the samples as shown in Fig. 1.

For HP-RS and HP-XRD measurements in powder or single crystal samples of $PbBi_2Te_4$, the samples were placed in a 250-μm-diameter hole performed in a stainless-steel gasket pre-indented to a thickness of 50 μm inside a membrane-driven diamond anvil cell (DAC) equipped with diamonds a culet of 500-μm-diameter. These HP experiments used a 4:1 methanol-ethanol (M-E) mixture as a pressure-transmitting medium (PTM). This medium is quasi-hydrostatic up to 10.5 GPa. Special attention was paid to avoid the sample bridging between the diamond anvils. Errandonea [40]

Structural characterization at HP was performed by means of angle-dispersive powder HP-XRD measurements at the BL04-MSPD beamline of the ALBA synchrotron, employing a monochromatic X-ray beam with $\lambda = 0.4246$ Å focused to 20 × 20 μm^2. Fauth et al. [41] The X-ray beam was focused by Kirkpartrick-Baez mirrors. XRD images were collected using a Rayonix SX165 CCD detector located at 240 mm from the sample. The detector parameters were calibrated using LaB_6 as standard. The two-dimensional diffraction images were integrated into one-dimensional profiles of intensity versus 2θ using Dioptas. Prescher and Prakapenka [42] XRD profiles were analyzed using the Le Bail method. In addition, Cu grains were loaded close to the sample in the HP-XRD experiments in order to use it as a pressure scale. Dewaele et al.

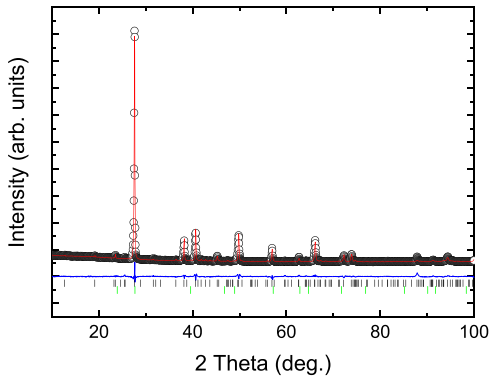

Fig. 1. XRD pattern measured at ambient conditions outside the DAC using $\lambda =$ 1.5406 Å. The black and green ticks indicate the Bragg positions of $PbBi_2Te_4$ and PbTe, respectively. The points are the results from experiments and the red is the Rietveld refinement. The blue line shows the difference. The R-values are R_p= 1.58 % and R_{wp}=2.45 %.

[43]

Vibrational characterization was carried out using polarized and unpolarized RS measurements at room conditions and HP to distinguish between the large number of phonons expected for this compound. All RS measurements were carried out with a Horiba Jobin Yvon LabRAM UV HR microspectrometer equipped with a thermoelectrically cooled multichannel CCD detector that allows a spectral resolution better than 2 cm^{-1}. The Raman signal was excited with a HeNe laser (632.8 nm line) with a power of less than 10 mW and collected in back-scattering geometry using a ULF Notch filter that allows obtaining signal down to 10 cm^{-1}. The frequencies of the Raman-active first-order phonons were obtained after fitting the Raman peaks with Voigt profiles of fixed Gaussian linewidth to the experimental setup resolution (1.6 cm^{-1}). For measuring the pressure, the ruby fluorescence scale was used. Mao et al. [44]

Hall-effect and resistivity measurements under pressure up to 13.35 GPa with an opposed anvils cell. We used steel-belted Bridgman tungsten carbide (WC) anvils with a tip of 15 mm in diameter. The samples were contained using two annealed pyrophyllite gaskets (0.5 mm thick each) in a split gasket geometry. The internal diameter of the gaskets was 5 mm. Hexagonal boron nitride (BN) was used as pressure-transmitting medium and also to electrically insulate the sample from the anvils. A 150-ton oil press was used to apply the load in the WC anvils. The sample was obtained by pre-compressing a fresh piece of $PbBi_2Te_4$ cut from the original sample. After this, the pre-compressed sample has a thickness of 50 μm thick. This sample was cut to have a surface of 2 mm $\times$ 2 mm. The pressure applied to the sample was determined by calibrating the load applied to the anvils against high-pressure resistivity transitions in calibrants. Errandonea et al. [45] The maximum pressure that can be achieved with this setup is 14 GPa. [46] Transport measurements were performed in a four-point configuration using silver (Ag) wires of 100 μm in diameter as electrical leads. To guarantee the good quality of contacts, the silver wires were flattened and sharpened at the tip, being soldered with high-purity indium to the sample. Hall effect measurements were conducted by applying alternatively a positive and a negative magnetic field (0.6 T). From the transport measurements, we obtained the pressure evolution of the resistivity, carrier concentration, and carrier mobility.

3. Theoretical calculations

Ab-initio calculations were performed within the density-functional theory (DFT) [47] using plane-wave basis-sets and the projector-augmented wave (PAW) [48,49] scheme with the Vienna ab-initio simulation package (VASP) package. Kresse and Hafner [50–52] The plane–wave kinetic–energy cutoff was defined with 400 eV in order to achieve highly converged results regarding the description of the electronic properties. Structure optimization is performed until the Hellman-Feynman forces on each atom are less than 10^{-3} eV/Å, while the energy convergence threshold is 10^{-5} eV. We have used the generalized–gradient approximation (GGA) for the exchange-correlation energy with the Perdew–Burke–Ernzerhof parametrization revised for solids (PBEsol). Perdew et al. [53] At each selected volume, the structures were fully relaxed to their equilibrium configuration through the calculation of the forces on atoms and the stress tensor with a dense special k–point sampling Monkhorst–Pack grids. Calculations of the electronic-band structures have been considered by employing spin-orbit coupling (SOC). In particular, the electronic band structures along high–symmetry directions and the corresponding electronic density of states (EDOS) were computed with a mesh of 18 $\times$ 18 $\times$ 18 k–points. The k-points path for the band structure calculations and the analysis of the DOS are carried out using VASPKIT. Wang et al. [54] The application of DFT-based calculations to the study of semiconductor properties under HP has been reviewed in the literature. Mujica et al. [55]

Lattice-dynamics calculations of phonon modes were performed at the zone center (Γ point) of the Brillouin zone. For the calculation of the dynamical matrix at Γ we used the direct force-constant approach (or supercell method), [51] using the Phonopy package, [56] which involves the calculation of all the atomic forces when each non–symmetry–related atom in the unit cell is displaced along non–symmetry–related directions.

The Bader analysis was performed by partitioning the PBEsol-DFT core and valence charge density grids. Tang et al. [57-60] A fine FFT grid was required to reproduce the correct total core charge accurately. The non–covalent interactions (NCI) of the PBEsol–DFT charge densities were computed using the NCI index. Johnson and Keinan [61,62] Such a tool defines a visualization index based on the electron density and its derivatives, enabling the identification of non–covalent interactions, based on the peaks that appear in the reduced density gradient at low densities.

4. Results and discussion

4.1. Structural properties under compression

$PbBi_2Te_4$ exhibits a rhombohedral crystal structure, described by space group $R\bar{3}m$, which is shown in Fig. 2. This structure can be described as a superposition of septuple atomic layers (Te-Bi-Te-Pb-Te-Bi-Te) along the c-axis in which a PbTe layer is inserted in the middle of a quintuple (Te-Bi-Te-Bi-Te) layer of Bi_2Te_3. Since both $PbBi_2Te_4$ and Bi_2Te_3 have a hexagonal unit cell that extends for three septuple layers along the c-axis, the insertion of the PbTe sublayer in each layer of Bi_2Te_3 leads to an increase of the *c* lattice parameter of $PbBi_2Te_4$ with respect to Bi_2Te_3, whereas the *a* lattice parameter remains almost constant and similar to that of Bi_2Te_3. Within the layers of $PbBi_2Te_4$, Pb and Bi are octahedrically coordinated by Te atoms as in their parent binary compounds PbTe and Bi_2Te_3 at room conditions. The octahedra are linked sharing edges forming 2D layers stacked along the *c* direction. The geometry of the two octahedra are slightly different. While the octahedron around Pb atoms is regular with the six Pb-Te distances being of equal length (around 3.162 Å), the octahedron around Bi atoms is not regular because it features two different Bi-Te distances, being the terminal Bi-Te distances (around 3.080 Å) much shorter than the internal ones (around 3.326 Å). Zhukova and Zaslavsky [23]

Fig. 1 shows a XDR pattern measured at ambient pressure before loading the sample in the DAC. Most peaks can be attributed to the known crystalline structure of $PbBi_2Te_4$. However, there are a few additional weak peaks that can be attributed to a very small amounts of PbTe (0.16 %). The Rietveld refinement of the XRD pattern to the structural model gives the following results for the lattice parameters for

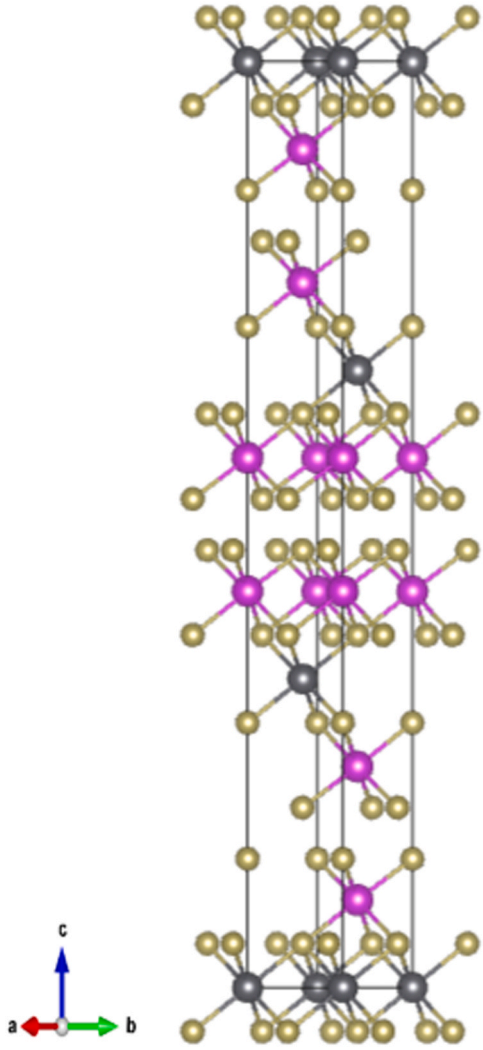

Fig. 2. $PbBi_2Te_4$ unit cell at ambient pressure. Grey, magenta, and brown colors correspond to Pb, Bi, and Te atoms, respectively.

$PbBi_2Te_4$: a = 4.442(1) Å and c = 41.778(4) Å. These values are consistent with the values reported in the literature. [20-23] The same can be said for the atomic positions which are summarized in Table 1. Results from present DFT simulations agree quite well with experiments. The calculated unit-cell parameters at 0 GPa are a = 4.435 Å and c = 41.555 Å and the atomic positions are summarized in Table 1.

Fig. 3 shows a selection of XRD patterns measured up to 10 GPa under compression and under decompression up to 0.7 GPa. The figure shows a Rietveld refinement of the XRD pattern measured at 1.1 GPa. In addition to the peaks from the sample, a peak from Cu (the pressure marker) is present in the XRD patterns. Up to 6.8 GPa the XRD pattern can be explained with the known rhombohedral structure of $PbBi_2Te_4$ by only changing the unit-cell parameters. At 7 GPa additional peaks appear indicating that changes occur in the sample. The additional peaks (the most intense are connected by lines in the figure) become stronger as pressure increases. In addition, the peaks of the ambient-pressure phase become weaker. The most intense peaks of the low-pressure phase are still present at 9.1 GPa (see for instance the peak denoted by an asterisk in Fig. 3) but disappear at 9.6 GPa. Above 9.1 GPa, a broad peak from the gasket becomes evident due to the closing of the gasket hole. All XRD patterns measured above 9.6 GPa cannot be indexed assuming only one crystal structure, not even with a triclinic space group. On the contrary, we found that these XRD patterns can be well fitted by the LeBail mehtod assuming the coexistence of PbTe and Bi_2Te_3 (see example of fit at 9.6 GPa in Fig. 3). For Bi_2Te_3 the structure is that of the high-pressure phase which is described by space group *C2/m* [63]. This result suggests that pressure induces a decomposition of $PbBi_2Te_4$. This hypothesis is supported by our DFT calculations since the total enthalpy of the decomposition products becomes smaller than the enthalpy of $PbBi_2Te_4$ at 8 GPa (see Fig. 4). The occurrence of decomposition is also supported by our Raman experiments as we will shown in the next section of this paper. The pressure-driven decomposition of $PbBi_2Te_4$ is analogous to the pressure-driven decomposition of $SnSb_2Te_4$ into SnTe and Sb_2Te_3 [15]. It should be noted here, than in recent study [64] it was proposed a structural phase transition, instead of decomposition, to explain changes observed in the XRD patters of $SnSb_2Te_4$. The proposed crystal structure, which was not supported by a structural refinement, is described by space group *C2/m*. However, such structure can never describe a compound with three formula units per unit cell (like $SnSb_2Te_4$ and $PbBi_2Te_4$), therefore is not correct. In addition, the unit-cell paramaters proposed for such monoclinic structure are identical to those of the high-pressure phase of Sb_2Te_3, which is also descriobed by space group *C2/m* [65]. Thus, the results reported by Ma *et al.* indeed confirm the pressure-driven decomposition of $SnSb_2Te_4$.

Table 1
Fractional atomic coordinates for $PbBi_2Te_4$. (Top) Present DFT calculations at 0 GPa and 0 K. (Bottom) Present experiment at room conditions. Experimental uncertainties are given in parentheses.

Atom	Wyckoff position	S.O.F.	x	y	z
Pb	3a	1	0.000	0.000	0.000
Bi	6c	1	0.000	0.000	0.428
Te1	6c	1	0.000	0.000	0.135
Te2	6c	1	0.000	0.000	0.287
Pb	3a	1	0.000	0.000	0.000
Bi	6c	1	0.000	0.000	0.429(4)
Te1	6c	1	0.000	0.000	0.133(1)
Te2	6c	1	0.000	0.000	0.285(2)

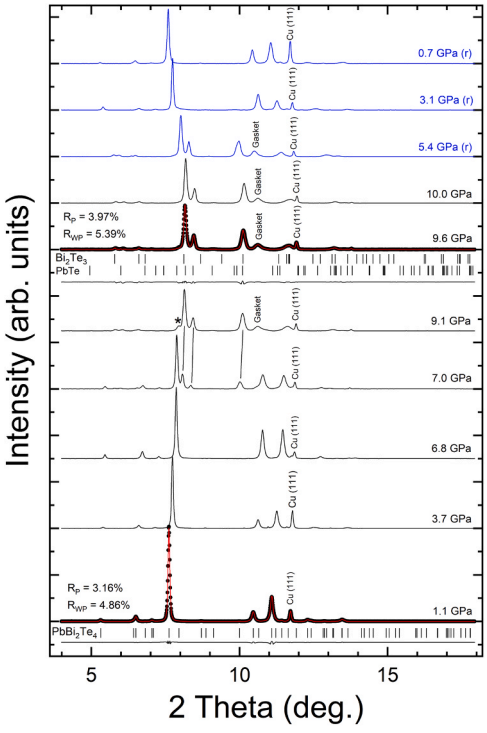

Fig. 3. HP-XRD patterns of $PbBi_2Te_4$ on compression up to 9.6 GPa. The pressures are indicated in the figure. R-values of the Rietveld and LeBail fits are included in the figure.

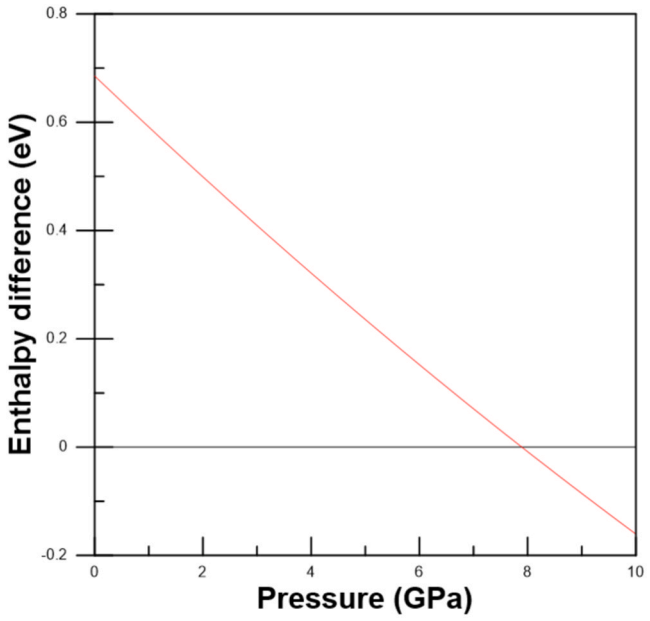

Fig. 4. Pressure dependence of the relative enthalpy of the decomposition products (PbTe and Bi_2Te_3, red line) with respect to $PbBi_2Te_4$ (black line).

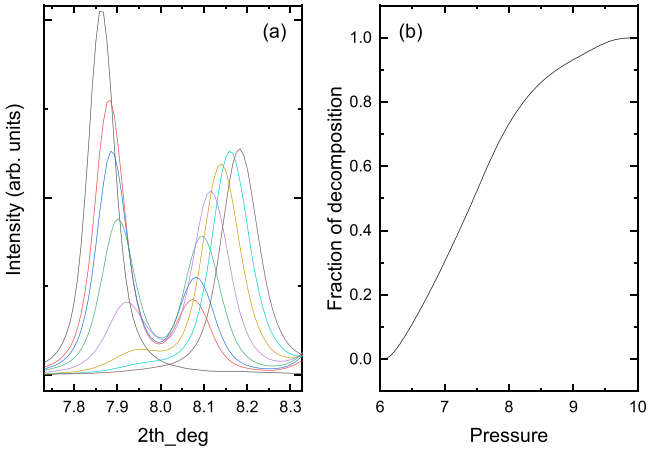

Fig. 5. (a) Zoom of the XRD pattern to highlight the gradual change of peak intensities in the $7.7 < 2\theta < 8.4$ region. The peak at lower angles is the strongest peak of $PbBi_2Te_4$ and the peak at higher angles is the strongest peak of the decomposition product. (b) Fraction of decomposition calculated using the intensity of peaks shown in (a) and the equation described in the text.

Upon decompression, we observe that the XRD patterns of the phases observed above 9 GPa are still present at 5.4 GPa. However, the XRD pattern of the original rhombohedral phase of $PbBi_2Te_4$ is obtained at 3.1 GPa and smaller pressures supporting the reversibility of the observed decomposition. The hysteresis in the reversion of decomposition could be related to the role played by kinetic barriers. Notice that the XRD pattern of the rhombohedral phase $PbBi_2Te_4$ at low pressures is similar to that of the rhombohedral phase of Bi_2Te_3 so they could be mistaken; however, despite the a lattice parameter of both compounds are similar, the lattice parameter c of $PbBi_2Te_4$ is ca. 42 Å while the corresponding one for Bi_2Te_3 is ca. 31 Å. Another fact we would like to highlight is that peak intensity ratios slightly between the profile under 1.1 GPa in the compression cycle and that under 0.7 GPa after decompression. The differences in intensities could be related to the presence of preferred orientations in the sample after decompression.

All in all the above results suggest the observation of a reversible pressure-induced decomposition in compressed $PbBi_2Te_4$. Notice that the pressure-induced chemical decomposition is usually an irreversible phenomenon since releasing pressure means decreasing the energy given to the system so no spontaneous chemical reaction is expected to occur in such conditions. However, the reversible decomposition of solids is possible according to thermodynamics. Hotta and Koga [66]. In fact, a partially reversible pressure-induced chemical decomposition has been recently reported in several compounds related to $PbBi_2Te_4$, e.g. $PbGa_2S_4$ [67] and $SnSb_2Te_4$. Sans et al. [15]. This phenomenon might be related to the large stability of the polyhedral units of the compounds that prevail after the pressure-induced decomposition. Further theoretical studies are needed to depper understand how pressure affects decomposition and confirm our hypothesis. However, they are beyond the scope of this study. We hope our results will trigger such studies.

The pressure-induced decomposition is gradual from 6.8 to 9.6 GPa. To quantify the amount of decomposition we have used the intensity of two peaks shown in Fig. 5(a) which can be assigned one to $PbBi_2Te_4$ and the another to the decomposition product. The fraction of decomposition is calculated using the quatient $I_{HP}/(I_{LP}+I_{HP})$, where I_{LP} is the intensity of the peak assigned to the low-pressure phase and I_{HP} is the intensity of the peak of the decomposition product. This quotient can be considered as the fraction of decomposition of $PbBi_2Te_4$. Errandonea et al. [68] The results are shown in Fig. 5(b). The figure shows that decomposition is gradual being only completed at 9.6 GPa. The observed observation provides an alternative explanation to the observation of superconductivity in $PbBi_2Te_4$ above 10 GPa [36] which was supported by resistivity measurements which were not complemented by XRD studies and were not supported by eletron-phonon coupling calculations. We propose that the observed superconductivity is not inherent to $PbBi_2Te_4$, but might be a result of pressure-induced decomposition. This is because, it is well documented that the high-pressure phase of Bi_2Te_3 stable at 10 GPa, which is described by space group $C2/m$ [69], and has been observed in our XRD and Raman experiments, is known to be superconducting. Zhang et al. [70] Interestingly, in the study of Matsumoto et al. [36] changes in the superconducting properties were observed at 21.7 GPa, which agrees with the critical superconducting pressure of PbTe. Brandt et al.[71] We consider that the agreement of the two critical pressure reported by Matsumoto et al. [36] with the superconducting temperatures of Bi_2Te_3 could not be a mere coincide, providing indirect support to the decomposition hypothesis. Future high-pressure superconducting studies on a homogeneous mixture of PbTe and Bi_2Te_3 are needed to confirm our hypothesis, but they are beyond the scope of this study.

From the XRD patterns, we have obtained the pressure dependence of unit-cell lattice parameters and unit-cell volume of the low-pressure phase of $PbBi_2Te_4$ (see Fig. 6). The results are reported up to 8.5 GPa because at higher pressure phase coexistence precludes an accurate determination of the unit-cell parameters. A good agreement between the experimental and theoretical results is observed. We have found that compression is not isotropic. Up to 2–3 GPa the c-axis is more compressible axis as a consequence of the weak interlayer bonding. This interlayer bonding is slightly stronger than the van der Waals forces typical of layered materials [72,73] because of the existence of intralayer non-conventional bonds, recently named electron-deficient multicenter bonds. Osman et al. [32,33] The compressibility pattern changes beyond 2–3 GPa since the a-axis becomes the most compressible axis above this pressure. This phenomenon is a consequence of the rapid change at low-pressure of the interlayer bonds, which rapidly become as hard as the intralayer bonds. This is a typical phenomenon of van der Waals layered compounds. Segura [74] The pressure dependence of the volume has been analyzed using a third-order Birch-Murnaghan equation of state (EOS) [75]. The obtained unit-cell volume at zero pressure (V_0), bulk modulus at zero pressure (B_0), and its pressure derivative (B_0') are summarized in Table 2. The fit of the EOS from experiments was performed using only the data collected under HP. Both calculations and experiments give nearly identical results. The V_0 obtained from the experiments performed in the DAC is 1 % smaller than the volume

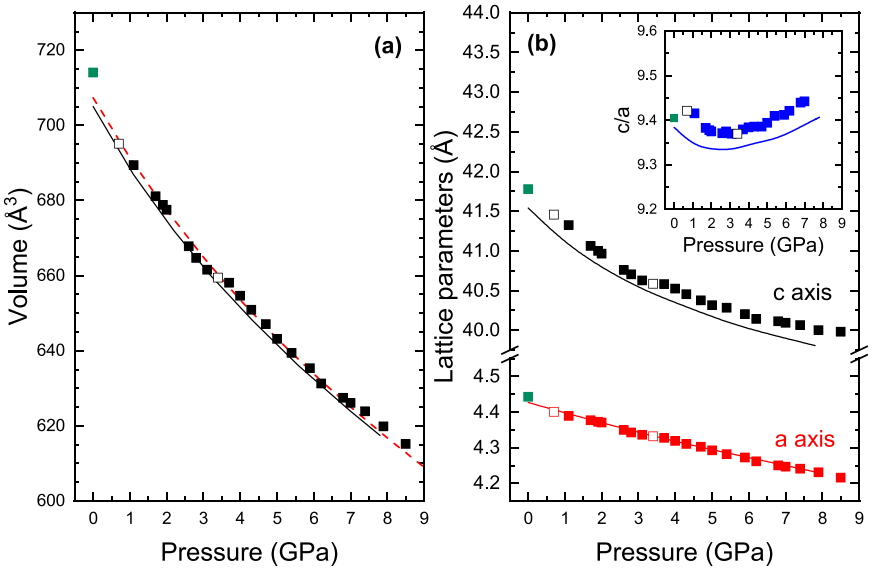

Fig. 6. Pressure dependence of the unit-cell volume (a) and lattice parameters (b). The inset shows the evolution of the c/a ratio with pressure. Solid lines represent the theoretically simulated data, solid (empty) squares are the experimental data obtained during compression (decompression). Green symbols represent the experiment at ambient pressure. The dashed red line in (a) is the EOS determined from experiments.

measured at ambient conditions with the sample outside the DAC. The small difference could be related to the use of two different set-ups. The bulk modulus is in the range of values reported for other layered tellurides, such as in Bi_2Te_3, [76], $SnSb_2Te_4$ and $SnSb_2Te_4$ (31–41 GPa), [15, 35] or GaGeTe (41–45 GPa) [77]. This means that the bulk modulus of $PbBi_2Te_4$ is dominated by the compressibility of the interlayer space as in other layered AB_2X_4 compounds. Sans et al. [15]

A consequence of the change in the compressibility of the two crystallographic axes around 3 GPa is the existence of a minimum of the c/a ratio in the 2–3 GPa range (see inset of Fig. 6). This ratio shows a clear change of tendency above 2 GPa similar to that observed experimental and theoretically in binary sesquichalcogenides with tetradymite structure α-Sb_2Te_3, α-Bi_2Te_3 and α-Bi_2Se_3, [78,79,65,63] and also in related ternary tetradymite-like compounds, such as $SnSb_2Te_4$ and $SnBi_2Te_4$. Vilaplana et al. [15,35] The big change in the slope of the c/a ratio in all these tetradymite-like compounds at HP is likely related to a pressure-induced isostructural phase transition (IPT) related to the hardening of the interlayer interactions. In other words, these layered compounds are prone to show an IPT of electronic origin as was already shown for $SnSb_2Te_4$. Sans et al. [15]

4.2. Vibrational properties under compression

$PbBi_2Te_4$ has a rhombohedral $R\bar{3}m$ structure, which contains in its primitive unit cell one formula unit (7 atoms). Therefore, according to group theory, $PbBi_2Te_4$ should have 21 vibrational modes at the Γ point with the mechanical representation: [80]

$$\Gamma = 3A_{1g} + 4A_{2u} + 4E_u + 3E_g \quad (1)$$

where E modes are doubly degenerated. From the 21 vibrational modes, there are 18 optical modes $3A_{1g} + 3A_{2u} + 3E_u + 3E_g$ and 3 acoustic modes ($A_{2u} + E_u$). The 18 vibrational modes are separated between Raman-active (gerade, g) and IR-active (ungerade, u) modes. Therefore, the 18 vibrational modes distribute as 6 Raman-active ($\Gamma_{Raman} = 3A_{1g} + 3E_g$) and 6 IR-active first-order modes ($\Gamma_{IR} = 3A_{2u} + 3E_u$). All six Raman-active modes have been theoretically calculated and reported in Table 3. However, only five Raman-active modes were theoretically predicted for $PbBi_2Te_4$ in a recent work. Mal et al. [24] Since the assignment of the 12 Raman-active and IR-active modes to atomic movements was recently done for isostructural $SnSb_2Te_4$ [15] through the Jmol Interface for Crystallographic and Electronic Properties (J-ICE), [81] we are going to use in this work the same notation for the different modes used in the work of rhombohedral $SnSb_2Te_4$.

To corroborate the results found in the structural study under pressure, we performed unpolarized HP-RS measurements. Fig. 7 shows the Raman spectrum of $PbBi_2Te_4$ on upstroke to 14 GPa and downstroke to 2.0 GPa. As can be observed, four of the six theoretically predicted Raman–active modes are observed at room pressure. Our Raman spectrum at room pressure is similar to that previously reported, [24] although our symmetry assignment of the different Raman-active modes is different. In particular, the predicted Raman mode with the lowest frequency (E_g^1 around 31 cm^{-1}) has not been observed neither by us nor by Mal et al. This is consistent with the small Raman cross-section of this mode in all tetradymites, as Bi_2Te_3. Kullmann et al. [82] Fortunately, the Raman spectra of $PbBi_2Te_4$ do not show the Raman modes attributed to Te clusters that were found in $SnSb_2Te_4$. Sans et al. [15,83] Given the

Table 2
EoS parameters (V_0, in Å^3, B_0, in GPa, and B_0' dimensionless) for $PbBi_2Te_4$ compound. Results obtained from present XRD experiments (XRD) and DFT calculations (DFT) are compared.

$PbBi_2Te_4$	V_0	B_0	B_0'
XRD	707.3(9)	41.5(6)	5.0(3)
DFT	705.4	41.9	4.9

Table 3
Theoretical (th.) and experimental (exp.) Raman-active frequencies at zero pressure (ω_0, in cm^{-1}) and pressure coefficients (a_1, in $cm^{-1}GPa^{-1}$; a_2, in $cm^{-1}GPa^{-2}$) in $PbBi_2Te_4$ according to fits to ω_0+a_1P+ a_2P^2. Uncertainties are given in parenthesis.

	$PbBi_2Te_4$ th.			$PbBi_2Te_4$ exp.		
Mode	ω_0	a_1	a_2	ω_0	a_1	a_2
E_g^1	31.0	2.4	−0.1			
A_{1g}^1	46.1	4.1	−0.2	48 (3)	3.4 (0.3)	−0.10 (0.04)
E_g^2	93.6	3.4	−0.1	93 (4)	3.0 (0.3)	0.00 (0.04)
E_g^3	109.2	4.2	−0.1	104 (4)	4.0 (0.4)	−0.09 (0.04)
A_{1g}^2	112.2	3.3	−0.1			
A_{1g}^3	139.5	3.5	0.0	130 (4)	3.4 (0.5)	−0.05 (0.06)

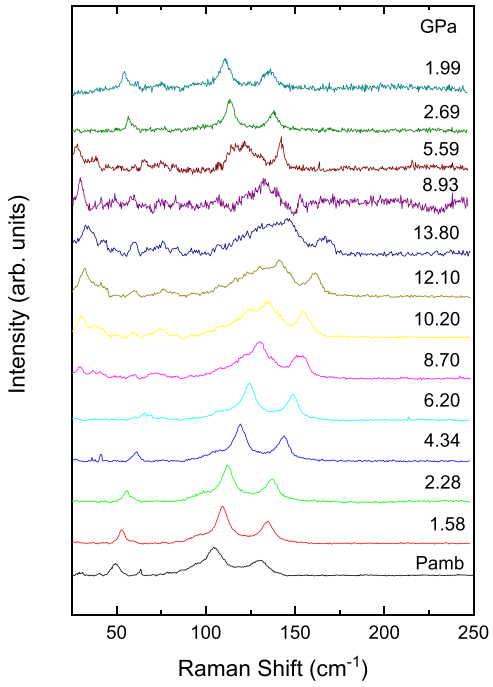

Fig. 7. Normalized Raman spectra of $PbBi_2Te_4$ at high pressure up to 13.8 GPa and decompression to 1.99 GPa.

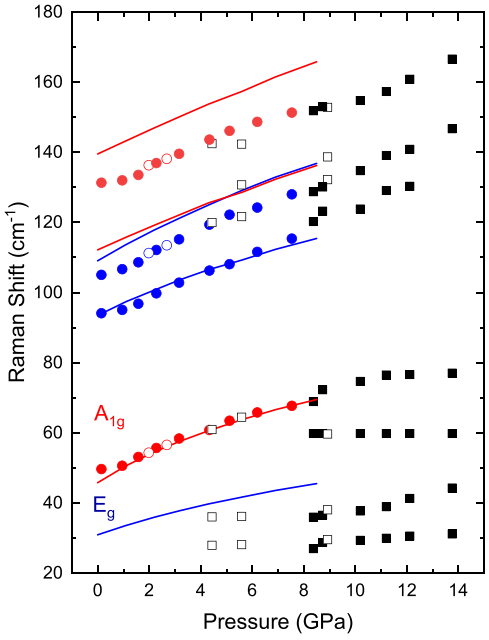

Fig. 8. Pressure dependence of the experimental (symbols) and theoretical (lines) Raman frequencies of $PbBi_2Te_4$ during compression and decompression. We use red color for A_{1g} modes, blue color for E_g modes, and black color for the mode of the HP phase. Solid symbols were measured during compression and empty symbols during decompression.

good agreement between the experimental and theoretical Raman–active mode frequencies (see also Table 3), we have tentatively assigned experimental Raman modes considering the predicted frequencies and pressure coefficients, as discussed below.

In layered materials vibrational modes at the Γ point can be classified into interlayer modes (in the low-frequency region) and intralayer modes (in medium- and high-frequency regions). Moreover, layered compounds crystallizing either in rhombohedral, hexagonal, or tetragonal space groups, show A (or B) and E modes. In rhombohedral $PbBi_2Te_4$, there are two pure interlayer modes (E_g^1 and A_{1g}^1), which have the lowest frequencies, and the other ten Raman and IR-active modes are intralayer modes distributed in both the medium and high–frequency ranges (see Table 3). The two interlayer modes, also known as rigid layer modes, correspond to out–of–phase movements of the neighbor layers both along the a–b plane (E_g^1 mode) and along the c–axis (A_{1g}^1 mode). Sans et al. [15]

The pressure dependence of the experimental and theoretical Raman–active modes in $PbBi_2Te_4$ (see Fig. 8 and Table 3) shows a good agreement of the experimental and theoretical frequencies within a 5 % accuracy interval. The only experimental mode whose assignment bears some doubts is the highest frequency mode measured at 130 cm^{-1}. We have tentatively attributed it to the theoretical A_{1g}^3 mode that is closer in frequency; however, it could happen that this mode is the A_{1g}^2 since both theoretical modes have similar pressure coefficients and a Raman mode has been experimentally found around 142 cm^{-1} at room conditions in an earlier work. Mal et al. [24]

It must be noted that our Raman results for $PbBi_2Te_4$ compare also nicely with the results for the isostructural compound $SnSb_2Te_4$ [15]. As expected, the frequencies of all modes in $PbBi_2Te_4$ are smaller than those of in $SnSb_2Te_4$ due to the larger masses of Pb and Bi than Sn and Sb, respectively. On the other hand, it can be observed that in both compounds the pressure coefficients at zero pressure (a_1) of the A_{1g} modes are larger than those of the E_g modes of similar frequency. This feature is characteristic of the larger increase of the interlayer forces with pressure than those of the intralayer forces and is consistent with the larger compressibility of the c-axis than that of the a-axis below 3 GPa previously commented.

Above 8 GPa, a clear change in the Raman spectra is observed that matches with the changes observed in XRD patterns above similar pressures, which we have related to a reversible decomposition. In particular, the Raman spectrum shows broadened bands leading to the observation of more Raman-active modes than those present at lower pressures before decomposition occurs. Those broad bands show two groups of Raman-active modes near 8 GPa. The low-frequency modes observed from 30 to 80 cm^{-1} and the high-frequency modes observed from 100 to 150 cm^{-1}. These two groups of Raman bands are consistent with those previously observed in the monoclinic $C2/m$ phase of beta-Bi_2Te_3. Vilaplana et al. [63] The broad bands observed from 100 to 150 cm^{-1} also coincide with the frequencies of the Raman modes of PbTe at the same pressures. Ves et al. [84] Therefore, we can conclude our HP-RS measurements confirm the pressure-induced decomposition observed by HP-XRD measurements.

On decreasing pressure from 14 GPa, we can observed that the same Raman spectra are found down to 5 GPa. However, a change of the Raman spectrum is found below 3 GPa. In particular the Raman spectrum at 2.0 GPa can be clearly identified as the one corresponding to the original rhombohedral structure of $PbBi_2Te_4$. Notice that the Raman spectrum of the rhombohedral phase $PbBi_2Te_4$ at low pressures only shows four Raman-active modes out of six predicted ones so it is easy to mistakenly interpret it as that of the rhombohedral phase of Bi_2Te_3; [63] however, the A_{1g}^1 Raman-active mode of $PbBi_2Te_4$ is observed more than 10 cm^{-1} lower in frequency than the A_{1g}^1 Raman-active mode of Bi_2Te_3. In summary, HP-RS measurements confirm the reversible pressure-induced decomposition of $PbBi_2Te_4$ observed in HP-XRD measurements. We would like to remark that the same hysteresis observed by XRD for the reversion of decomposition is found by Raman experiments.

4.3. Transport properties under compression

$PbBi_2Te_4$ is a narrow band gap semiconductor with an indirect band gap around 0.23 eV [85] and a n-type conductivity. Kuznetsova et al.

[21,28,22,29] Resistance of $PbBi_2Te_4$ has been reported at pressures as a function of temperature in line with the discovery of pressure-induced superconductivity; [36] however, the resistivity at room temperature as a function of pressure has not been reported in $PbBi_2Te_4$. Fig. 9 shows the pressure dependence of the resistivity (ρ), carrier concentration (n), and carrier mobility (μ) of $PbBi_2Te_4$ as obtained from our resistivity and Hall-effect measurements up to 13.4(1) GPa. The resistivity at ambient pressure is comparable to that previously reported. Matsumoto et al. [36] Thus, our results are consistent with the n-type semiconductor and narrow band gap of that $PbBi_2Te_4$. The value of $9 \times 10^{-3}\Omega \cdot$ cm is compatible with an intrinsic semiconductor with a band-gap energy close to 0.2 eV. Up to 6 GPa there is slight increase in the electron mobility and a slight decrease of the carrier concentration. The second phenomenon leads to a gradual decrease of resistivity. Above 6 GPa, there are pronounced changes of both carrier concentration and mobility that cause a sharp decrease of resistivity up to 10.5 GPa. The value of resistivity above 10.5 GPa is consistent with a metallic behavior. The carrier concentration and electrical resistivity remain nearly constant under pressures above 10.5 GPa. This is consistent with a metallic behavior. In metals the resistivity is slightly affected by pressure in contrast to the behavior of semiconductors. Ezenwa and Yoshino [86]

In order to interpret the above results, we performed ab initio DFT calculations of the electronic band structure at pressures between 0 and 10 GPa. The electronic band structures of $PbBi_2Te_4$ at 0 and 8 GPa are shown in Fig. 10, where the top valence band and the lowermost conduction band are highlighted. At room pressure, the valence band maximum occurs at Γ point and the conduction band minimum lies along the Γ–Z direction. Therefore, our simulations suggest that $PbBi_2Te_4$ is a narrow band gap semiconductor with an indirect band gap of 0.175 eV at ambient conditions, in good agreement with previous calculations at room pressure. Zhang and Singh [30,36,87-89,29] As pressure increases above 1 GPa, the valence band maximum shift to a point along the Γ–L direction so there is a new indirect bandgap. Therefore, the absolute indirect bandgap has a negligible change with increasing pressure up to 10 GPa, much like the change of the direct

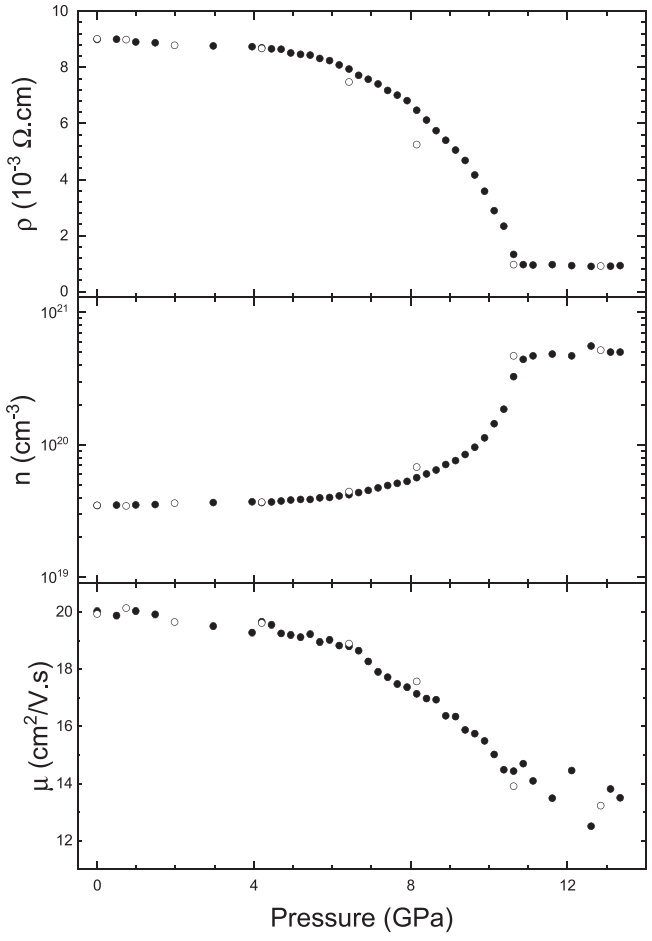

Fig. 9. Resistivity, carrier concentration, and carrier mobility of $PbBi_2Te_4$ at room temperature as a function of pressure. Solid symbols were measured during compression and empty symbols during decompression.

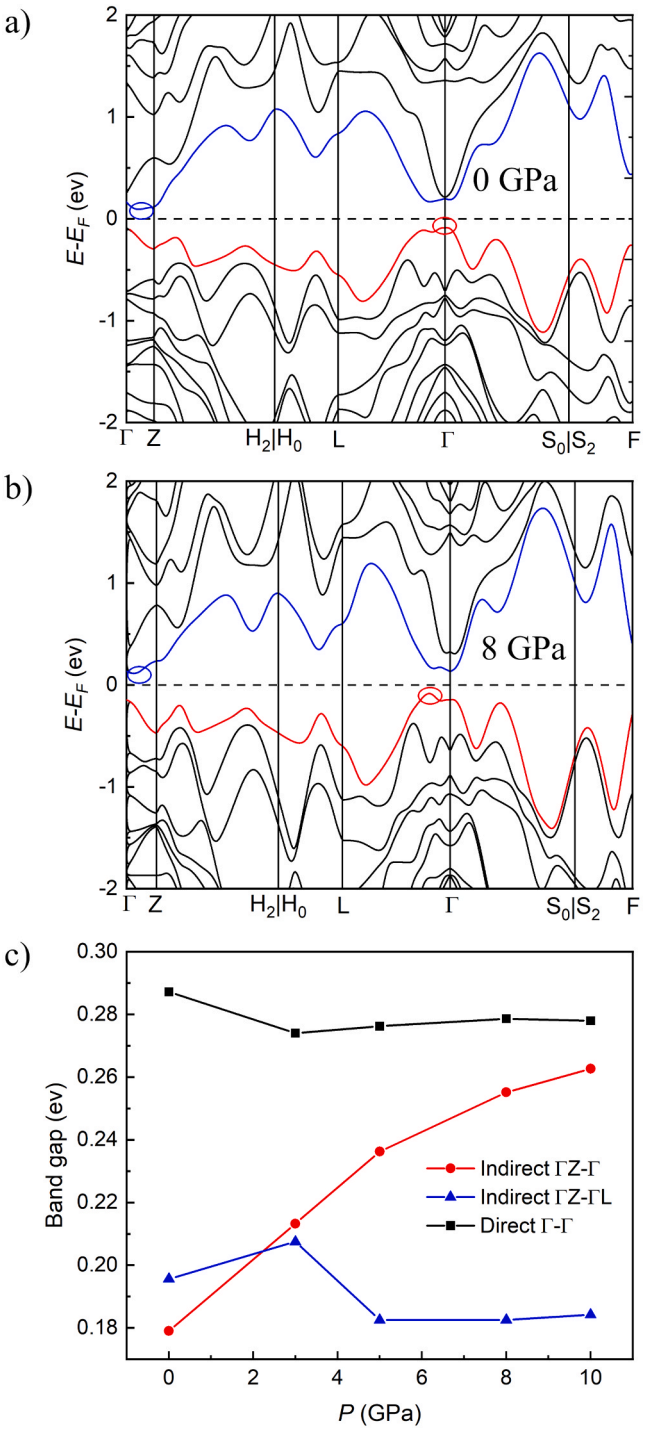

Fig. 10. Electronic band structure of $PbBi_2Te_4$ at 0 GPa (a) and 8 GPa (b). The topmost valence band and the lowermost conduction bands are plotted in red and blue colors, respectively.(c) Pressure dependence of the smallest direct and indirect bandgaps in the tetradymite-like phase.

bandgap at the Γ point. These changes of the different bandgaps with increasing pressure are plotted in Fig. 10. The small changes of the direct and absolute indirect bandgap of the tetradymite-like phase of $PbBi_2Te_4$ with increasing pressure results in the maintenance of the strong topological insulating character of the compound up to the maximum pressure according to the calculated Z_2 indices ν_0 (ν_1, ν_2,ν_3) = 1(1,1,1) according to VASP2TRACE software of the Bilbao Crystallographic Server. Vergniory et al. [90–92] This result is in contrast to the results of other tetradymite-like compounds, such as β-As_2Te_3, that loose the topological properties on increasing pressure. Vilaplana et al. [73]

The experimental results imply a decrease of the bandgap energy above 6 GPa [93] that does not occur according to our calculations. This means that the decrease of the resistivity above 6 GPa is consistent with a metallic behavior that does not correspond to the theoretical results for the tetradymite-like phase. Notice that the pressure dependence of ρ in $PbBi_2Te_4$ is different from that reported for $SnBi_2Te_4$ and $SnSb_2Te_4$, which are p-type semiconductors. Pan et al. [28,15,35]

Therefore, the changes observed in the transport properties of $PbBi_2Te_4$ above 6 GPa are consistent with the decomposition of $PbBi_2Te_4$ observed in HP-XRD and HP-RS experiments. Notice that Bi_2Te_3 undergoes a semiconductor-to-metal transition above 8–10 GPa due to the phase transition from the rhombohedral R-3m to the monoclinic C2/m phase. Einaga et al. [94,95] This is the same pressure range in which the onset of metallization is observed in our experiments. In particular, the decrease of the carrier mobility is consistent with the formation of defects in the sample leading to an enhancement of electron scattering by ionized defects. Errandonea et al. [96] The change of slope of the mobility at about 6 GPa would correspond to a change of the dominant carrier scattering mechanism. When increasing further the pressure there are no important changes caused in the transport properties. All changes induced by pressure in the transport are reversible supporting the reversibility of the pressure-induced decomposition already observed in HP-XRD and HP-RS measurements.

Interestingly, the observed pressure-induced decomposition above ca. 6–9 GPa according to our HP-XRD, HP-RS, and HP-transport measurements allows us to give a reasonable explanation for the previously observed pressure-induced superconductivity of $PbBi_2Te_4$ above this pressure range. Matsumoto et al. [36] Note that superconductivity was reported to occur in $PbBi_2Te_4$ at 10 GPa, pressure at which we have shown there is a mixture of the decomposition products PbTe and Bi_2Te_3. Moreover, a critical temperature around 2–3 K was observed at 10–13 GPa in good agreement with the 2.8 K critical temperature found in the $C2/m$ phase of Bi_2Te_3 at 10.2 GPa. Nakayama et al. [79,94] Consequently, the superconductivity in $PbBi_2Te_4$ at 10 GPa can be explained by the observed pressure-induced superconductivity in Bi_2Te_3 above 7 GPa. Matsubayashi et al. [97] Interestingly, Matsumoto et al. measured a change in the slope of the pressure dependence of the superconducting temperature at 16 GPa [36] and this pressure coincides with the onset of superconductivity in PbTe. Brandt et al. [71] Therefore, the reported results on pressure-induced superconductivity in $PbBi_2Te_4$ are fully consistent with the pressure-driven decomposition reported here so superconductivity cannot be ascribed to $PbBi_2Te_4$ but to their decomposition products, in particular to the $C2/m$ phase of Bi_2Te_3.

A similar explanation to that already given for the observation of pressure-induced superconductivity in $PbBi_2Te_4$ can likely be given for the observation of pressure-induced superconductivity in other AB_2X_4 compounds, e.g. $GeSb_2Te_4$, [98] $SnSb_2Te_4$, [38,64] and $GeBi_2Te_4$. Liu et al. [37] In particular, a pressure-induced decomposition has been also observed in $SnSb_2Te_4$ and suggested to occur in $SnBi_2Te_4$, [15] and the lattice parameters found for the $C2/m$ phase of $SnSb_2Te_4$ above 6 GPa [15,64] are very similar to those already reported for the $C2/m$ phases of Sb_2Te_3 and Bi_2Te_3. Zhu et al. [65,99] Moreover, the possibility of a pressure-induced decomposition in $GeBi_2Te_4$ has been already suggested by Liu et al. [37] On the other hand, we have to stress that pressure-induced superconductivity was not observed on upstroke in the rhombohedral phase of $GeSb_2Te_4$ but only once after decompression from the body-centered cubic (BCC) phase. Greenberg et al. [98] Note that the BCC phase is a disorderded phase with mixed cations and anions that has been already found in all tetradymite-like sesquichalcogenides at HP [100,69,99] and that it is quenchable at room conditions in $GeSb_2Te_4$. Kalkan et al. [101] Therefore, pressure-induced superconductivity in $GeSb_2Te_4$ can be likely ascribed to the quenched disordered BCC phase; the same phase that is observed in tetradymite sesquichalcogenides at HP.

4.4. Chemical bonding in $PbBi_2Te_4$

To finish the paper, we want to comment on the different types of chemical bonding present in $PbBi_2Te_4$. As already commented, there are two main types of chemical bonds in layered materials, the intralayer and the interlayer bonds. The interlayer bonds in common layered materials are typically considered to be weak bonds of van der Waals (vdW) type. This type of bonds is observed e.g. in III-VI layered compounds, such as InSe, GaSe, and GaS, and in transition metal chalcogenides AX_2 (A=W, Mo; X=S, Se, Te). In contrast, recent studies have revealed that interlayer bonds in tetradymite-like V_2VI_3 sesquichalcogenides, such as Bi_2Se_3, Bi_2Te_3, Sb_2Te_3, and beta-As_2Te_3, show a stronger interlayer bonding that is reflected in the smaller interlayer space in tetradymite-like compounds than what is expected for common vdW materials. Wang et al. [72,102,103,73,104] In other words, the typical van der Waals interlayer bonding is strengthened due to the presence of additional electronic charge in the interlayer space coming from the intralayer bonds. This extra interlayer charge is caused by the partial delocalization of electrons present in intralayer bonds and it is related to the non-conventional character of the intralayer bonding in these and other phase change materials, such as rocksalt-like IV-VI compounds. Wuttig et al. [72,105] This non-conventional bonding in phase change materials has been discussed in the recent years to be explained by two models: the hypervalent and the metavalent bonding models. Wuttig et al. [106,107,6]. However, it has recently been suggested that these materials feature an old kind of bond that was till now thought to be not possible in electron-rich elements, the electron-deficient multicenter bond. Osman et al. [32,33]

In order to show the electron-deficient character of the intralayer bonding in $PbBi_2Te_4$, we have theoretically calculated the number of electrons shared (ES) between the Pb-Te and Bi-Te atoms inside the septuple atomic layers according to the Quantum Theory of Atoms in Molecules. Richard and Bader [72,33,108] At 0 GPa, the calculated ES values for Pb-Te2, Bi-Te2, and Bi-Te1 are 0.91, 0.93, and 1.14, respectively. In comparison the corresponding ES values for Sn-Te2, Sb-Te2, and Sb-Te1 in $SnSb_2Te_4$ are 0.88, 0.91, and 1.4, respectively. In a prior work on $SnSb_2Te_4$, we showed that the Sb-Te1 bonds were considered be slightly modified covalent bonds, while the Sn-Te2 and Sb-Te2 bonds are not covalent bonds but unconventional bonds that were considered to be metavalent; [15] i.e. they can be catalogued as electron-deficient multicenter bonds according to the revised notation. Osman et al. [32,33]

The comparison of the ES values of the Pb-Te2 and Bi-Te2 bonds in $PbBi_2Te_4$ with their corresponding Sn-Te2 and Sb-Te2 bonds in $SnSb_2Te_4$ suggest that all these bonds are electron-deficient multicenter bonds. On the other hand, the much lower ES value of the Bi-Te1 bond in $PbBi_2Te_4$ than that of its corresponding Sb-Te1 bond in $SnSb_2Te_4$ suggest that the former bond is already an electron-deficient multicenter bond unlike the later. This result is consistent with the occurrence of the electron-deficient multicenter bonds in the heavier elements of the group. Osman et al. [33] The appearance of more defined electron-deficient multicenter bonds in the compounds with the heaviest elements is also consistent with the appearance of topological insulating properties in the compounds with the heaviest elements, such as tellurides instead than in selenides, as it is the case of $PbBi_2Se_4$ vs. $SnBi_2Se_4$. Menshchikova et al. [87] Moreover, the covalent character and the

electron-deficient multicenter character (previously considered to be metavalent) of the different intralayer bonds is consistent with the location of the different bonds in the ES vs. ET map, being ET the renormalized number of electrons transferred between the two bonded atoms, if we consider that Pb-Te2, Bi-Te2, Bi-Te1, Sn-Te2, Sb-Te2, and Sb-Te1 have ET values around 0.25(5). Wuttig et al. [6,33] This is also consistent with the observation of these unconventional bonds in tetradymite-like pnictogen sesquichalcogenides. Cheng et al. [72,73]

While the electron-deficient character of the intralayer bonds in $PbBi_2Te_4$ is reflected in the low ES values of the Pb-Te2, Bi-Te1, and Bi-Te2 bonds as compared to covalent bonds with ES values well above 1.5, [6,33] the multicenter character of the intralayer bonds in $PbBi_2Te_4$ is reflected in the hypercoordinated (sixfold) Pb and Bi cations and the linear Te-Pb-Te and Te-Bi-Te bonds in three dimensions. Osman et al. [33] Notice that normally coordinated (fourfold) Ge and Sb cations with angular covalent bonds occur in glassy $GeSb_2Se_4$ [109] and intermediate hypercoordinated (fivefold) Sn and Sb cations, with a mixture of covalent and electron-deficient multicenter bonds in two dimensions similar to that present in TlI, InI, and InBr, [33] is found in $SnSb_2Se_4$. Smith and Parise [110] Therefore, it can be concluded that the increase of hypercoordination, and therefore of multicenter character along different spatial directions, increases when heavier elements participate in AB_2X_4 compounds, being the tetradymite-like structures those having the largest number (three) of electron-deficient multicenter bonds (linear anion-cation-anion bonds) around each cation.

Finally, it must be stressed that our calculations for $PbBi_2Te_4$ and $SnSb_2Te_4$ do not show a significant change of the ES and ET values as pressure increases (up to 10 GPa) as long as the low-pressure rhombohedral structure is maintained. Therefore, we conclude that the main intralayer bonds in these layered tetradymite-like compounds are electron-deficient multicenter bonds irrespective to the pressure. In this context, it must be observed that despite all the intralayer bonds are electron-deficient multicenter bonds, the bond with the larger covalent character is the Bi-Te1 bond that has the larger ES value. The larger ES value of the Bi-Te1 bond than of the Bi-Te2 at 0 GPa is consistent with the shorter length of the Bi-Te1 bond (3.080 Å) than for the Bi-Te2 bond (3.326 Å) since covalent bonds are shorter that multicenter bonds, irrespective of they being electron-rich or electron-deficient. As expected, an even shorter Bi-Te1 bond length (3.075 Å) is found in $SnBi_2Te_4$ since a much larger covalent character of this bond is expected for the tetradymite-like compounds with lighter elements. In summary, the presece of intralayer bonds with electron-deficient multicenter character explains the delocalized character of some electrons that contribute to strengthen the interlayer bonds in these tetradymite-like layered materials in contrast to common layered vdW compounds.

5. Conclusions

We have reported a joint experimental and theoretical study of the topological insulator and thermoelectric material $PbBi_2Te_4$ in which its structural, vibrational, and electric properties have been studied under compression. The results of powder X-ray diffraction, Raman scattering, and transport measurements have been explained thanks to the help of state-of-the-art ab initio calculations. In addition to reporting the equation of state of the rhombohedral phase and the pressure dependence of the Raman-active phonons and transport properties, we have found that this compound retains the topological properties of the rhombohedral tetradymite-like phase up to its reversible pressure-induced decomposition into its parent materials (PbTe and Bi_2Te_3) in the range from 6 to 9 GPa. This decomposition allows us to explain the observed pressure-induced superconductivity in this and related compounds with tetradymite-like structures since the same type of pressure-induced superconductivity has been previously observed in tetradymite-like sesquichalcogenides (Sb_2Te_3, Bi_2Te_3, and Bi_2Se_3). In addition, we have clarified the different nature of the interlayer and intralayer bonding in these materials in comparison with other layered chalcogenides, emphasizing that the extraordinary properties of the tetradymite-like phase of $PbBi_2Te_4$ are related to the existence of electron-deficient multicenter bonds in this material as well as in its parent PbTe and Bi_2Te_3 compounds.

CRediT authorship contribution statement

Alfonso Muñoz: Investigation, Formal analysis. **Placida Rodriguez-Hernandez:** Investigation, Formal analysis. **Juán Ángel Sans:** Investigation. **Francisco Javier Manjón:** Writing – review & editing, Writing – original draft, Validation, Investigation, Funding acquisition, Formal analysis, Conceptualization. **Tania Garcia Sanchez:** Writing – review & editing, Writing – original draft, Investigation, Formal analysis. **Vanesa Paula Cuenca-Gotor:** Investigation. **Hussien H. Osman:** Investigation, Formal analysis. **Samuel Gallego-Parra:** Investigation. **Catalin Popescu:** Investigation. **Oliver Oeckler:** Investigation. **Daniel Errandonea:** Writing – review & editing, Writing – original draft, Validation, Investigation, Funding acquisition, Formal analysis.

Declaration of Competing Interest

There are no conflicts of interest to declare.

Data Availability

No data was used for the research described in the article.

Acknowledgements

This publication is financed by Spanish Ministerio de Ciencia e Innovacion and the Agencia Estatal de Investigacion MCIN/AEI/10.13039/501100011033 as part of the project MALTA Consolider Team network (RED2022–134388-T), and I+D+i projects PID2021–125927NB-C21 and PID2022–138076NB-C41/C42/C44 co-financed by EU FEDER funds and by project PROMETEO CIPROM/2021/075 (GREENMAT) financed by Generalitat Valenciana. This study also forms part of the Advanced Materials program supported by MCIN with funding from European Union NextGenerationEU (PRTR-C17.I1) and by Generalitat Valenciana through projects MFA/2022/007 (MAT-GREEN) and MFA/2022/025 (ARCANGEL). T.G.-S. thanks Universitat Politecnica de Valencia for the support through the program “Ayudas para la recualificacion del profesorado universitario”, financial support provided by Ministerio de Universidades, funding from the European Union-Next generation EU. T.G.-S. and V.P.C.-G. thanks Primeros proyectos de investigacion 2022 (PAID-06–22), en el marco de ayudas del Vicerrectorado de Investigacion de la Universitat Politecnica de Valencia. The authors also thank the ALBA synchrotron light source for providing beamtime under proposal number 2021085226. S.G.P. acknowledges PRACE for awarding access to the Fenix Infrastructure resources at CINECA, which are partially funded by the European Union s Horizon 2020 research and innovation program through the ICEI project under the grant agreement No. 800858. We also acknowledge the computer resources of the Centro de Supercomputación de Castilla y León (SCAYLE)”.

References

[1] M.I. Eremets, V.S. Minkov, A.P. Drozdov, P. Kong, V. Ksenofontov, S.I. Shylin, S. L. Bud’ko, R. Prozorov, F.F. Balakirev, D. Sun, et al., High-temperature superconductivity in hydrides: experimental evidence and details, J. Supercond. Nov. Magn. 35 (2022) 965–977.
[2] C. Felser, X.L. Qi, Topological insulators, MRS Bull. 39 (2014) 843–846.
[3] M.A. Green, A. Ho-Baillie, H.J. Snaith, The emergence of perovskite solar cells, Nat. Photon. 8 (2014) 506–514.
[4] A. Hayat, P. Zareapour, S.Y.F. Zhao, A. Jain, I.G. Savelyev, M. Blumin, Z. Xu, A. Yang, G. Gu, H.E. Ruda, et al., Hybrid high-temperature-superconductor–semiconductor tunnel diode, Phys. Rev. X 2 (2012) 041019.

[5] M. Kulbak, D. Cahen, G. Hodes, How important is the organic part of lead halide perovskite photovoltaic cells? Efficient $CsPbBr_3$ cells, J. Phys. Chem. Lett. 6 (2015) 2452–2456.

[6] M. Wuttig, C.F. Schön, J. Lötfering, P. Golub, C. Gatti, J.Y. Raty, Revisiting the nature of chemical bonding in chalcogenides to explain and design their properties, Adv. Mater. 35 (2023) 2208485.

[7] Oosawa, Y., Tateno, Y., Mukaida, M., Tsunoda, T., Imai, Y., Isoda, Y., Nishida, I., 1999. $PbBi_2Te_4$ and $PbBi_4Te_7$, Thermoelectric Materials in the System of Pb-Bi-Te, In: Eighteenth International Conference on Thermoelectrics. Proceedings, ICT'99 (Cat. No. 99TH8407), IEEE.550-553.

[8] L. Shelimova, O. Karpinskij, V. Zemskov, P. Konstantinov, E. Avilov, M. Kretova, Promising thermoelectric materials, based on laminated tetradimito-like chalcogenides, Perspekt. Mater. 5 (2000) 23–32.

[9] D. Pesin, A.H. MacDonald, Spintronics and pseudospintronics in graphene and topological insulators, Nat. Mater. 11 (2012) 409–416.

[10] Y. Chen, J.G. Analytis, J.H. Chu, Z. Liu, S.K. Mo, X.L. Qi, H. Zhang, D. Lu, X. Dai, Z. Fang, et al., Experimental realization of a three-dimensional topological insulator, Bi_2Te_3, Science 325 (2009) 178–181.

[11] M.Z. Hasan, C.L. Kane, Colloquium: topological insulators, Rev. Mod. Phys. 82 (2010) 3045.

[12] D. Hsieh, Y. Xia, D. Qian, L. Wray, J. Dil, F. Meier, J. Osterwalder, L. Patthey, J. Checkelsky, N.P. Ong, et al., A tunable topological insulator in the spin helical dirac transport regime, Nature 460 (2009) 1101–1105.

[13] A. Mellnik, J. Lee, A. Richardella, J. Grab, P. Mintun, M.H. Fischer, A. Vaezi, A. Manchon, E.A. Kim, N. Samarth, et al., Spin-transfer torque generated by a topological insulator, Nature 511 (2014) 449–451.

[14] X.L. Qi, S.C. Zhang, Topological insulators and superconductors, Rev. Mod. Phys. 83 (2011) 1057.

[15] J.A. Sans, R. Vilaplana, E.L. DaSilva, C. Popescu, V.P. Cuenca-Gotor, A. Andrada-Chacón, J. Sánchez-Benitez, O. Gomis, A.L. Pereira, P. Rodríguez-Hernández, et al., Characterization and decomposition of the natural Van der Waals $SnSb_2Te_4$ under compression, Inorg. Chem. 59 (2020) 9900–9918.

[16] A. Aghazade, Phase relations and characterization of solid solutions in the $SnBi_2Te_4$-$PbBi_2Te_4$ and $SnBi_4Te_7$-$PbBi_4Te_7$ systems, Azerbaijan Chem. J. (2022) 75–80.

[17] K. Kase, I. Kusachi, S. Kishi, Rucklidgeite solid-solution in the Yanahara deposit, Japan, Can. Mineral. 31 (1993) 99.

[18] J. Rucklidge, Frohbergite, montbrayite, and a new Pb-Bi telluride, Can. Mineral. 9 (1969) 709–716.

[19] Y.N. Zav'yalov, V. Begizov, Rucklidgeite, $(Bi, Pb)_3Te_4$, a new mineral from the zod and kochkar gold-ore deposits, Int. Geol. Rev. 19 (1977) 1451–1456.

[20] O. Karpinskii, L. Shelimova, E. Avilov, M. Kretova, V. Zemskov, X-ray diffraction study of mixed-layer compounds in the PbTe–Bi_2Te_3 system, Inorg. Mater. 38 (2002) 17–24.

[21] L. Kuznetsova, V. Kuznetsov, D. Rowe, Thermoelectric properties and crystal structure of ternary compounds in the Ge (Sn, Pb) Te–Bi_2Te_3 systems, J. Phys. Chem. Solids 61 (2000) 1269–1274.

[22] L. Shelimova, O. Karpinskii, P. Konstantinov, E. Avilov, M. Kretova, V. Zemskov, Crystal structures and thermoelectric properties of layered compounds in the ATe–Bi_2Te_3 (A= Ge, Sn, Pb) systems, Inorg. Mater. 40 (2004) 451–460.

[23] T. Zhukova, A. Zaslavsky, Crystal structures of the compounds$PbBi_4Te_7$, $PbBi_2Te_4$, $SnBi_4Te_7$, $SnBi_2Te_4$, $SnSb_2Te_4$, and $GeBi_4Te_7$, Kristallografiya 16 (1971) 918–922.

[24] P. Mal, G. Bera, G. Turpu, S.K. Srivastava, A. Gangan, B. Chakraborty, B. Das, P. Das, Vibrational spectra of $Pb_2Bi_2Te_3$, $PbBi_2Te_4$, and $PbBi_4Te_7$ topological insulators: temperature-dependent Raman and theoretical insights from DFT simulations, Phys. Chem. Chem. Phys. 21 (2019) 15030–15039.

[25] C. Lee, J.N. Kim, J.Y. Tak, H.K. Cho, J.H. Shim, Y.S. Lim, M.H. Whangbo, Comparison of the electronic and thermoelectric properties of three layered phases Bi_2Te_3, $PbBi_2Te_4$ and $PbBi_4Te_7$: Lego thermoelectrics, AIP Adv. 8 (2018) 115213.

[26] W. Ma, J. Tian, P. Boulet, M.C. Record, First-principle investigations on the electronic and transport properties of $PbBi_2Te_2X_2$ (X= S/Se/Te) monolayers, Nanomaterials 11 (2021) 2979.

[27] P. Mal, B. Das, A. Lakhani, G. Bera, G. Turpu, C. Tomy, P. Das, Transport evidence of linear Dirac dispersion of non-trivial surface states in Fe-substituted $PbBi_2Te_4$ 3d topological insulator, Phys. E Low. Dimens. Syst. Nanostruct. 130 (2021) 114672.

[28] L. Pan, J. Li, D. Berardan, N. Dragoe, Transport properties of the $SnBi_2Te_4$–$PbBi_2Te_4$ solid solution, J. Solid State Chem. 225 (2015) 168–173.

[29] L. Zhang, D.J. Singh, Electronic structure and thermoelectric properties: $PbBi_2Te_4$ and related intergrowth compounds, Phys. Rev. B 81 (2010) 245119.

[30] W. Ma, M.C. Record, J. Tian, P. Boulet, Strain effects on the electronic and thermoelectric properties of n(PbTe)-m (Bi_2Te_3) system compounds, Materials 14 (2021) 4086.

[31] J.H. Yim, K. Jung, H.J. Kim, H.H. Park, C. Park, J.S. Kim, Effect of composition on thermoelectric properties in PbTe-Bi_2Te_3 composites, J. Electron. Mater. 40 (2011) 1010–1014.

[32] F.J. Manjón, H.H. Osman, M. Savastano, Á. Vegas, Electron-Deficient Multicenter Bonding in Phase Change Materials: A Chance for Reconciliation, ChemRxiv (2024), https://doi.org/10.26434/chemrxiv-2024-0qbj7.

[33] H.H. Osman, A. Otero-de-laRoza, P. Rodríguez-Hernández, A. Muñoz, F. J. Manjón, Metavalent Multicenter Bonding in Pnictogens and Chalcogens: Nature and Mechanism of Formation. ChemRxiv (2023) https://doi.org/10.26434/chemrxiv-2023-pv66p-v2.

[34] W.P. Hsieh, P. Zalden, M. Wuttig, A.M. Lindenberg, W.L. Mao, High-pressure raman spectroscopy of phase change materials, Appl. Phys. Lett. 103 (2013) 191908.

[35] R. Vilaplana, J. Sans, F. Manjón, A. Andrada-Chacón, J. Sánchez-Benítez, C. Popescu, O. Gomis, A. Pereira, B. García-Domene, P. Rodríguez-Hernández, et al., Structural and electrical study of the topological insulator $SnBi_2Te_4$ at high pressure, J. Alloy. Compd. 685 (2016) 962–970.

[36] R. Matsumoto, Z. Hou, M. Nagao, S. Adachi, H. Hara, H. Tanaka, K. Nakamura, R. Murakami, S. Yamamoto, H. Takeya, et al., Data-driven exploration of new pressure-induced superconductivity in $PbBi_2Te_4$, Sci. Technol. Adv. Mater. 19 (2018) 909–916.

[37] C. Liu, Y. Gao, C. Tian, C. Jiang, C. Zhu, X. Wu, X. Huang, T. Cui, Pressure-driven dome-shaped superconductivity in topological insulator $GeBi_2Te_4$, J. Phys. Condens. Matter 36 (2024) 225703.

[38] P. Song, R. Matsumoto, Z. Hou, S. Adachi, H. Hara, Y. Saito, P. Castro, H. Takeya, Y. Takano, Pressure-induced superconductivity in $SnSb_2Te_4$, J. Phys. Condens. Matter 32 (2020) 235901.

[39] O. Oeckler, M.N. Schneider, F. Fahrnbauer, G. Vaughan, Atom distribution in $SnSb_2Te_4$ by resonant X-ray diffraction, Solid State Sci. 13 (2011) 1157–1161.

[40] D. Errandonea, High-pressure phase transitions and properties of MTO_4 compounds with the monazite-type structure, Phys. Status Solidi (B) 254 (2017) 1700016.

[41] F. Fauth, I. Peral, C. Popescu, M. Knapp, The new material science powder diffraction beamline at alba synchrotron, Powder Diffr. 28 (2013) S360–S370.

[42] C. Prescher, V.B. Prakapenka, Dioptas: a program for reduction of two-dimensional X-ray diffraction data and data exploration, High. Press Res. 35 (2015) 223–230.

[43] A. Dewaele, P. Loubeyre, M. Mezouar, Equations of state of six metals above 94 GPa, Phys. Rev. B 70 (2004) 094112.

[44] H. Mao, J.A. Xu, P. Bell, Calibration of the ruby pressure gauge to 800 kbar under quasi-hydrostatic conditions, J. Geophys. Res. Solid Earth 91 (1986) 4673–4676.

[45] D. Errandonea, D. Martínez-García, A. Segura, J. Ruiz-Fuertes, R. Lacomba-Perales, V. Fages, A. Chevy, L. Roa, V. Mũnoz-SanJosé, High-pressure electrical transport measurements on p-type gase and inse, High. Press. Res. 26 (2006) 513–516.

[46] A. Segura, J. Sans, D. Errandonea, D. Martinez-Garcia, V. Fages, High conductivity of ga-doped rock-salt zno under pressure: hint on deep-ultraviolet-transparent conducting oxides, Appl. Phys. Lett. 88 (2006) 011910.

[47] P. Hohenberg, W. Kohn, Inhomogeneous electron gas, Phys. Rev. 136 (1964) B864.

[48] P.E. Blöchl, Projector augmented-wave method, Phys. Rev. B 50 (1994) 17953.

[49] G. Kresse, D. Joubert, From ultrasoft pseudopotentials to the projector augmented-wave method, Phys. Rev. b 59 (1999) 1758.

[50] G. Kresse, J. Furthmüller, Efficiency of ab-initio total energy calculations for metals and semiconductors using a plane-wave basis set, Comput. Mater. Sci. 6 (1996) 15–50.

[51] G. Kresse, J. Hafner, Ab initio molecular dynamics for liquid metals, Phys. Rev. B 47 (1993) 558.

[52] G. Kresse, J. Hafner, Ab initio molecular-dynamics simulation of the liquid-metal–amorphous-semiconductor transition in germanium, Phys. Rev. B 49 (1994) 14251.

[53] J.P. Perdew, A. Ruzsinszky, G.I. Csonka, O.A. Vydrov, G.E. Scuseria, L. A. Constantin, X. Zhou, K. Burke, Restoring the density-gradient expansion for exchange in solids and surfaces, Phys. Rev. Lett. 100 (2008) 136406.

[54] V. Wang, N. Xu, J.C. Liu, G. Tang, W.T. Geng, Vaspkit: A user-friendly interface facilitating high-throughput computing and analysis using vasp code, Comput. Phys. Commun. 267 (2021) 108033.

[55] A. Mujica, A. Rubio, A. Munoz, R. Needs, High-pressure phases of group-IV, III–V, and II–VI compounds, Rev. Mod. Phys. 75 (2003) 863.

[56] A. Togo, First-principles phonon calculations with phonopy and phono3py, J. Phys. Soc. Jpn. 92 (2023) 012001.

[57] G. Henkelman, A. Arnaldsson, H. Jónsson, A fast and robust algorithm for bader decomposition of charge density, Comput. Mater. Sci. 36 (2006) 354–360.

[58] E. Sanville, S.D. Kenny, R. Smith, G. Henkelman, Improved grid-based algorithm for bader charge allocation, J. Comput. Chem. 28 (2007) 899–908.

[59] W. Tang, E. Sanville, G. Henkelman, A grid-based bader analysis algorithm without lattice bias, J. Phys.: Condens. Matter 21 (2009) 084204.

[60] M. Yu, D.R. Trinkle, Accurate and efficient algorithm for bader charge integration, J. Chem. Phys. 134 (2011) 064111.

[61] J. Contreras-García, E.R. Johnson, S. Keinan, R. Chaudret, J.P. Piquemal, D. N. Beratan, W. Yang, Nciplot: a program for plotting noncovalent interaction regions, J. Chem. Theory Comput. 7 (2011) 625–632.

[62] E. Johnson, S. Keinan, Mori- Sánchez, P.; Contreras- García, J.; Cohen, A.J.; Yang, W. Revealing noncovalent interactions, J. Am. Chem. Soc. 132 (2010) 6498–6506.

[63] R. Vilaplana, O. Gomis, F. Manjón, A. Segura, E. Pérez-González, P. Rodríguez-Hernández, A. Muñoz, J. González, V. Marín-Borrás, V. Muñoz-Sanjosé, et al., High-pressure vibrational and optical study of Bi_2Te_3, Phys. Rev. B 84 (2011) 104112.

[64] Y. Ma, H. Wang, R. Li, H. Liu, J. Zhang, X. Wang, Q. Jing, X. Wang, W. Dong, J. Chen, et al., Pressure-induced superconductivity in $SnSb_2Te_4$, Microstructures 4 (2024) 2024012.

[65] S. Souza, C. Poffo, D. Trichês, J. De Lima, T. Grandi, A. Polian, M. Gauthier, High pressure monoclinic phases of Sb_2Te_3, Phys. B: Condens. Matter 407 (2012) 3781–3789.

[66] M. Hotta, N. Koga, Extended kinetic approach to reversible thermal decomposition of solids: A universal description considering the effect of the gaseous product and the kinetic compensation effect, Thermochim. Acta 733 (2024) 179699.

[67] T. Garcia-Sanchez, S. Gallego-Parra, A. Liang, J.L. Rodrigo-Ramon, A. Muñoz, P. Rodriguez-Hernandez, J. Gonzalez-Platas, J.Á. Sans, V.P. Cuenca-Gotor, H. H. Osman, et al., Joint experimental and theoretical study of $PbGa_2S_4$ under compression, J. Mater. Chem. C. 11 (2023) 11606–11619.

[68] D. Errandonea, R. Boehler, S. Japel, M. Mezouar, L. Benedetti, Structural transformation of compressed solid ar: an x-ray diffraction study to 114 GPa, Phys. Rev. B 73 (2006) 092106.

[69] F.J. Manjón, R. Vilaplana, O. Gomis, E. Pérez-González, D. Santamaría-Pérez, V. Marín-Borrás, A. Segura, J. González, P. Rodríguez-Hernández, A. Muñoz, et al., High-pressure studies of topological insulators Bi_2Se_3, Bi_2Te_3, and Sb_2Te_3, Phys. Status Solidi (B) 250 (2013) 669–676.

[70] J. Zhang, S. Zhang, H. Weng, W. Zhang, L. Yang, Q. Liu, S. Feng, X. Wang, R. Yu, L. Cao, et al., Pressure-induced superconductivity in topological parent compound Bi_2Te_3, Proc. Natl. Acad. Sci. 108 (2011) 24–28.

[71] N. Brandt, D. Gitsu, N. Popovich, V. Sidorov, S. Chudinov, Superconductivity of the compounds pbte and pbse under high pressure, Jetp Lett. 22 (1975) 104–106.

[72] Y. Cheng, O. Cojocaru-Mirédin, J. Keutgen, Y. Yu, M. Küpers, M. Schumacher, P. Golub, J.Y. Raty, R. Dronskowski, M. Wuttig, Understanding the structure and properties of sesqui-chalcogenides (ie, V_2VI_3 or Pn_2Ch_3 (Pn= pnictogen, Ch= chalcogen) compounds) from a bonding perspective, Adv. Mater. 31 (2019) 1904316.

[73] R. Vilaplana, S. Gallego-Parra, E.L. daSilva, D. Martínez-García, G. Delaizir, A. Muñoz, P. Rodríguez-Hernández, V. Cuenca-Gotor, J. Sans, C. Popescu, et al., Experimental and theoretical study of β -As_2Te_3 under hydrostatic pressure, J. Mater. Chem. C 11 (2023) 1037–1055.

[74] A. Segura, Layered indium selenide under high pressure: a review, Crystals 8 (2018) 206.

[75] F. Birch, Finite elastic strain of cubic crystals, Phys. Rev. 71 (1947) 809.

[76] A. Polian, M. Gauthier, S.M. Souza, D.M. Trichês, J.C. de Lima, T.A. Grandi, Two-dimensional pressure-induced electronic topological transition in Bi_2Te_3, Phys. Rev. B 83 (2011) 113106.

[77] E. Bandiello, S. Gallego-Parra, A. Liang, J. Sans, V. Cuenca-Gotor, E.L. daSilva, R. Vilaplana, P. Rodríguez-Hernández, A. Muñoz, D. Diaz-Anichtchenko, et al., Structural, vibrational, and electronic behavior of two gagete polytypes under compression, Mater. Today Adv. 19 (2023) 100403.

[78] O. Gomis, R. Vilaplana, F. Manjón, P. Rodríguez-Hernández, E. Pérez-González, A. Muñoz, V. Kucek, C. Drasar, Lattice dynamics of Sb_2Te_3 at high pressures, Phys. Rev. B 84 (2011) 174305.

[79] A. Nakayama, M. Einaga, Y. Tanabe, S. Nakano, F. Ishikawa, Y. Yamada, Structural phase transition in Bi_2Te_3 under high pressure, High. Press. Res. 29 (2009) 245–249.

[80] E. Kroumova, M. Aroyo, J. Perez-Mato, A. Kirov, C. Capillas, S. Ivantchev, H. Wondratschek, Bilbao crystallographic server: useful databases and tools for phase-transition studies, Ph. Transit 76 (2003) 155–170.

[81] P. Canepa, R.M. Hanson, P. Ugliengo, M. Alfredsson, J-ice: a new jmol interface for handling and visualizing crystallographic and electronic properties, J. Appl. Crystallogr. 44 (2011) 225–229.

[82] W. Kullmann, J. Geurts, W. Richter, N. Lehner, H. Rauh, U. Steigenberger, G. Eichhorn, R. Geick, Effect of hydrostatic and uniaxial pressure on structural properties and Raman active lattice vibrations in Bi_2Te_3, Phys. Status Solidi (b) 125 (1984) 131–138.

[83] F.J. Manjón, S. Gallego-Parra, P. Rodriguez-Hernandez, A. Munoz, C. Drasar, V. Munoz-Sanjose, O. Oeckler, Anomalous Raman modes in tellurides, J. Mater. Chem. C 9 (2021) 6277–6289.

[84] S. Ves, Y.A. Pusep, K. Syassen, M. Cardona, Raman study of high pressure phase transitions in PbTe, Solid State Commun. 70 (1989) 257–260.

[85] K. Kuroda, H. Miyahara, M. Ye, S. Eremeev, Y.M. Koroteev, E. Krasovskii, E. Chulkov, S. Hiramoto, C. Moriyoshi, Y. Kuroiwa, et al., Experimental verification of $PbBi_2Te_4$ as a 3d topological insulator, Phys. Rev. Lett. 108 (2012) 206803.

[86] I.C. Ezenwa, T. Yoshino, Electrical resistivity of Cu and Au at high pressure above 5 GPa: Implications for the constant electrical resistivity theory along the melting curve of the simple metals, Materials 14 (2021) 5476.

[87] T.V. Menshchikova, S.V. Eremeev, Y.M. Koroteev, V.M. Kuznetsov, E.V. Chulkov, Ternary compounds based on binary topological insulators as an efficient way for modifying the dirac cone, JETP Lett. 93 (2011) 15–20.

[88] I. Shvets, I.I. Klimovskikh, Z.S. Aliev, M. Babanly, J. Sánchez-Barriga, M. Krivenkov, A.M. Shikin, E.V. Chulkov, Impact of stoichiometry and disorder on the electronic structure of the $PbBi_2T_{4-x}Se_x$ topological insulator, Phys. Rev. B 96 (2017) 235124.

[89] L.L. Wang, Highly tunable band inversion in AB_2X_4 (A= Ge, Sn, Pb; B= As, Sb, Bi; X= Se, Te) compounds, Phys. Rev. Mater. 6 (2022) 094201.

[90] Vergniory, M., Elcoro, L., Felser, C., Regnault, N., Bernevig, B., Wang, Z., 2018. The (High Quality) Topological Materials in the world.arXiv preprint arXiv: 1807.10271.

[91] M. Vergniory, L. Elcoro, C. Felser, N. Regnault, B.A. Bernevig, Z. Wang, A complete catalogue of high-quality topological materials, Nature 566 (2019) 480–485.

[92] M.G. Vergniory, B.J. Wieder, L. Elcoro, S.S. Parkin, C. Felser, B.A. Bernevig, N. Regnault, All topological bands of all nonmagnetic stoichiometric materials, Science 376 (2022) eabg9094.

[93] A. Liang, P. Rodriguez-Hernandez, A. Muñoz, S. Rahman, A. Segura, D. Errandonea, Pressure-dependent modifications in the optical and electronic properties of Fe $(IO_3)_3$: the role of Fe 3d and I 5p lone–pair electrons, Inorg. Chem. Front. 8 (2021) 4780–4790.

[94] M. Einaga, Y. Tanabe, A. Nakayama, A. Ohmura, F. Ishikawa, Y. Yamada, New superconducting phase of Bi_2Te_3 under pressure above 11 GPa, J. Phys. Conf. Ser. 215 (2010) 012036.

[95] J. Zhang, C. Liu, X. Zhang, F. Ke, Y. Han, G. Peng, Y. Ma, C. Gao, Electronic topological transition and semiconductor-to-metal conversion of Bi_2Te_3 under high pressure, Appl. Phys. Lett. 103 (2013) 052102.

[96] D. Errandonea, E. Bandiello, A. Segura, J. Hamlin, M. Maple, P. Rodriguez-Hernandez, A. Muñoz, Tuning the band gap of $PbCrO_4$ through high-pressure: evidence of wide-to-narrow semiconductor transitions, J. Alloy. Compd. 587 (2014) 14–20.

[97] K. Matsubayashi, T. Terai, J. Zhou, Y. Uwatoko, Superconductivity in the topological insulator Bi_2Te_3 under hydrostatic pressure, Phys. Rev. B 90 (2014) 125126.

[98] E. Greenberg, B. Hen, S. Layek, I. Pozin, R. Friedman, V. Shelukhin, Y. Rosenberg, M. Karpovski, M. Pasternak, E. Sterer, et al., Superconductivity in multiple phases of compressed $GeSb_2Te_4$, Phys. Rev. B 95 (2017) 064514.

[99] L. Zhu, H. Wang, Y. Wang, J. Lv, Y. Ma, Q. Cui, Y. Ma, G. Zou, Substitutional alloy of bi and te at high pressure, Phys. Rev. Lett. 106 (2011) 145501.

[100] M. Einaga, A. Ohmura, A. Nakayama, F. Ishikawa, Y. Yamada, S. Nakano, Pressure-induced phase transition of Bi_2Te_3 to a bcc structure, Phys. Rev. B 83 (2011) 092102.

[101] B. Kalkan, S. Sen, S. Clark, Nature of phase transitions in crystalline and amorphous GeTe-Sb2Te3 phase change materials, J. Chem. Phys. 135 (2011) 124510.

[102] B.J. Kooi, M. Wuttig, Chalcogenides by design: functionality through metavalent bonding and confinement, Adv. Mater. 32 (2020) 1908302.

[103] E.L. daSilva, M.C. Santos, P. Rodríguez-Hernández, A. Muñoz, F.J. Manjón, Theoretical study of pressure-induced phase transitions in Sb_2S_3, Bi_2S_3, and Sb_2Se_3, Crystals 13 (2023) 498.

[104] R. Wang, F.R. Lange, S. Cecchi, M. Hanke, M. Wuttig, R. Calarco, 2d or not 2d: strain tuning in weakly coupled heterostructures, Adv. Funct. Mater. 28 (2018) 1705901.

[105] M. Wuttig, V.L. Deringer, X. Gonze, C. Bichara, J.Y. Raty, Incipient metals: functional materials with a unique bonding mechanism, Adv. Mater. 30 (2018) 1803777.

[106] J. Hempelmann, P.C. Müller, L. Reitz, R. Dronskowski, Quantum chemical similarities of bonding in polyiodides and phase-change materials, Inorg. Chem. 62 (2023) 20162–20171.

[107] M. Wuttig, C.F. Schön, D. Kim, P. Golub, C. Gatti, J.Y. Raty, B.J. Kooi, Á. M. Pendás, R. Arora, U. Waghmare, Metavalent or hypervalent bonding: is there a chance for reconciliation? Adv. Sci. 11 (2024) 2308578.

[108] F. Richard, R. Bader. Atoms in Molecules: A Quantum Theory, 1990.

[109] R. Svoboda, D. Brandová, J. Málek, Crystallization behavior of $GeSb_2Se_4$ chalcogenide glass, J. Non-Cryst. Solids 388 (2014) 46–54.

[110] P.P. Smith, J.B. Parise, Structure determination of $SnSb_2S_4$ and $SnSb_2Se_4$ by high-resolution electron microscopy, Acta Crystallogr. Sect. B Struct. Sci. 41 (1985) 84–87.